University of Szeged

Doctoral School of Multidisciplinary Medical Science

Biophysical investigations of single cells with optically actuated microtools

Summary of the Ph.d thesis of

Tamás Fekete

Supervisor

Dr. Lóránd Kelemen

Biological Research Centre of Szeged, Biophysics institute

Szeged

2021

I. Introduction and aims

To target biological barriers such as the Blood brain barrier (BBB) it is crucial to understand its behavior and its function. This cumbersome task would be easier if we had more knowledge about its physicochemical and mechanical properties.

In my thesis I demonstrate the possibility to utilize optical tweezers-based (OT) micromanipulation techniques to obtain information on BBB constituent endothelial cells. For this, I rely on tailor-designed, task-specific microtools as probes, which I fabricated with two-photon polymerization (TPP) out of SU-8 photoresist and actuated with the optical tweezers.

1. First, I measured the Young's modulus of living human cerebral microvascular endothelial cells (hCMEC/D3) with high precision and found that the OT-based results are comparable to those published in the literature.
    - Designing a task-specific microtool for cell indentation experiments
    - Create an arrangement for the measurements where the cells located on a vertical wall
    - Determination the Young moduli for hCMEC cells with our new OT-based measurement method using optically actuated microtools

2. Second, I investigated the highly effective nanoparticle targeting ligand glutathione adhesion force onto the surface of living endothelial cells
    - Creation of an effective PEG-meditated functionalization protocol to immobilize GSH on SU-8 surfaces
    - Determination of the GSH coverage with fluorescent microscopy
    - Characterization of binding probability of GSH-functionalized, optically trapped ellipsoids to four different types of cells
    - Measuring adhesion forces of GSH-covered SU-8 surface towards endothelial cells via our new OT-based method

II. Materials and methods

1. SU-8 structures and two photon polymerization

In all experiments the microstructures were made out of SU-8 photopolymer spin-coated into thin layers on top of a cover slide. SU-8 is a biocompatible, chemically inert resist which has high mechanical strength and high refractive index. For cell supporting walls SU-8 2075 was used to reach approximately 100 µm tall structures, and for the fabrication UV-mask lithography were used. For the manipulators and the blocks ~16 µm thick SU-82007 was used and made via two photon polymerization (TPP) for great precision. TPP is a reliable method for microfabrication of micrometer sized objects out of photosensitive materials.

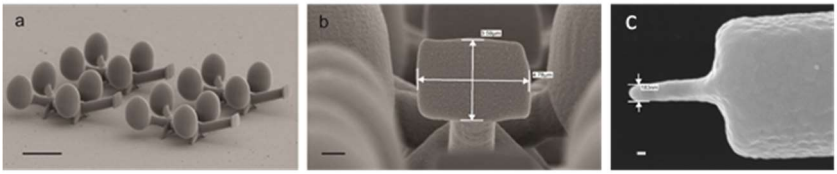

Figure 1. Scanning electron microscopy images of the micromanipulators. ***(a)*** *Structures of the micromanipulators scalebar: 10 µm.* ***(b)*** *Parameters of the contact surface. scalebar: 1 µm.,* ***(c)*** *pointy ended microtool's tip scale 100 nm*

2. Microstructure functionalization

To measure binding force between the cells and the optically manipulated structures, I had to functionalize the TPP fabricated objects with the ligand of interest, glutathione (GSH). First, I show how the GSH can be linked on the SU-8 surface covalently. To modify SU-8's surface, first we have to open the surface epoxy-rings which leaves activated carboxyl-groups on SU-8 surface (**Step I.**). In the following step, carboxyl on the SU-8 can react the with the free primary amine-groups of the amino-PEG-maleimide (**Step II.**). The surface treated until this step was later used as one of the **controls** and we refer to it as a **PEGylated** surface. To cover the surface with GSH

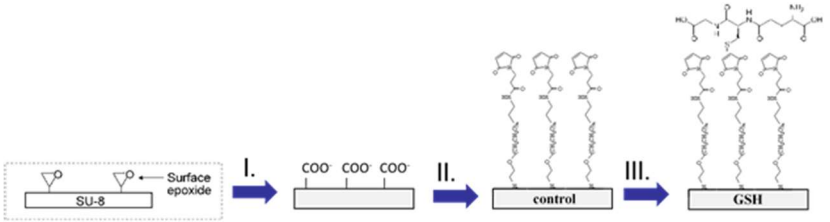

Figure 2. Significant steps of GSH functionalization protocol

I simply used PBS solution of 100 mM GSH; the thiol-group of this ligand molecule reacts with the maleimide part of the linker to form oxime-ether connection (**PEG-GSH** sample) (**Step III.**).

To visualize and to prove the GSH presence on SU-8 surface I used amine-reactive CY-5-ester dye to stain the primary amine of the GSH molecules. The CY-5 staining was carried out after all three functionalization steps on the TPP-made blocks, also including a PEG-bisamine-coated sample. They were observed with a wide-field fluorescent and a confocal microscope.

3. Cell cultures

In all experiments, we used cells which are composing the blood-brain barrier: primary rat brain astroglia, pericyte, and endothelial cells (RBEC), as well as cultured human cerebral microvascular endothelial cells (hCMEC/D3 cell line). To help cell adhesion to the SU-8 walls and the glass substrate, we applied adhesion promoters such as Matrigel, rat tail collagen and *poly-L-lysin.* Moreover, a home-made sample holder was used with a PID-controlled heater element to guarantee the 37 °C for the cells under the optical tweezer measurements.

4. Holographic optical tweezer-based measurements

For the cell stiffness measurement as well as for the binding and adhesion force experiments, I used our HOT system. In the binding probability experiments with ellipsoids, I was using just one focal spot, but for the adhesion force and the cell stiffness measurements I had to create 4 focal spots for the microtool, what could be manipulated with high precision and accuracy. The focal spots, that trap the manipulators' spheres are generated with a spatial light modulator (SLM) and could be moved with 6 degrees of freedom. Furthermore, to obtain indentation or adhesion forces from the measurements, the stiffness of the used microtools was determined.

The trap stiffness of the indentation experiment's micromanipulator was 16.49±2 pN/μm and that of the adhesion force measurements was 25.8±2 pN/μm. The deviation between the two kinds of manipulator stiffness originates from the slightly different diameter of the trapping spheres of the two manipulators.

4.1: Cell indentation experiments

In these experiments hCMEC/D3 cells were used that were grown on SU-8 walls made by mask lithography onto a circular coverslide substrate, and the manipulators approached the cells that grew on the vertical parts of the scaffold in a perpendicular direction. As a first step, the microtools were collected with a pipette form their cover slide and placed into the well containing the cells (Step 1 of *Figure 3.*). At this point, the microtools were randomly scattered nearby the supporting walls. An individual tool was trapped with the optical tweezer and elevated from the horizontal glass substrate by about ~10 µm moving the trapping microscope objective. Then, the microtools were aligned by moving the optical traps such that the plane of their four spheres are perpendicular to the optical axis, and then with stationary optical traps the sample stage was moved to approximate a cell to about 1-2 µm (Step 2). Then with a fixed stage the manipulator was turned towards the target cell by rotating the optical traps, until the tool's tip pointed towards the supporting wall (Step 3). At this point, a fine tuning of the manipulator's position was executed: the cell's silhouette was brought into focus together with the manipulator's tip by moving the focusing objective. At Step 4 the indentation experiment was executed by moving the held structure with only the HOT by an average speed of 0.05 µm/s and with 10 nm steps toward the cells, and in every step a bright field image of the manipulator was recorded.

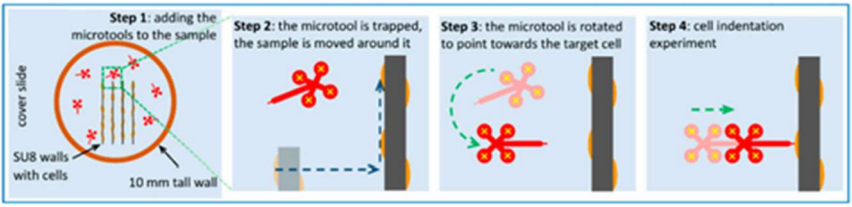

Figure 3. Schematic of the indentation experiment: Microtools being pipetted into the sample well (Step 1) their alignment towards the target cell; yellow crosses mark the trapping beams positions, blue arrows indicate sample stage translations (Step 2) and green arrows the optical trap actuations (Step 3-4)

Before the tool's tip made a contact with the cell or the wall (in the control experiments), the position of the structure's spheres and that of the optical traps were coincided, but when the tip reached the target, the movement of the trapping beams continued for about another 1 µm while the manipulator's position was retarded relative them.

To determine the cells' Young's modulus, the force that pushes the microstructure to the target cell and the cell's indentation need to be determined; for both values, the microtool's position has to be measured precisely. The force was calculated from the displacement of the microstructure relative to the trapping foci. The indentation was determined from the difference of the microtools' position when they were pushed against the cells and against an uncovered SU-

8 wall. The difference in the movements in these two instances provided the indentation value as described later.

4.2 Adhesion force measurements

In these experiments the RBEC and hCMEC/D3 cells were grown similarly on a vertical supporting wall, the preparations for the micromanipulators and the approximation (with 100 nm stepsize) of the cells happened similarly as described earlier. When it touched the cell, which was determined visually, the manipulator was pushed further against it by less than a micrometer to exert few tens of pN pushing force on the target cell. When the micromanipulator is pushed to the chosen cells surface, ΔX (the difference between the T trap position and M center of mass of the trapped sphere) is negative. After 10 seconds of waiting, we pulled the structure backwards with 250 nm or 50 nm steps which resulted in different retraction speeds: 0.5 µm/s and 0.1 µm/s, respectively.

At the beginning of the retraction, the microtool does not move but the still negative ΔX slowly increases. If there is no adhesion between the micromanipulator and the cell, ΔX first becomes zero, then the microtool detaches from the cell and follows the trapping foci. If there is any cellular interaction, ΔX becomes positive, and a considerable pulling force is exerted on the microtool by the optical tweezer. Eventually, when the optical force becomes greater than the adhesion force, the microtool separates from the cell's surface and the centers of the trapped spheroids return to the trap positions (ΔX becomes zero). Next, either the same microtool was used to test another cell (maximum of 3 measurements per microtool) or another microtool was used on the next cell.

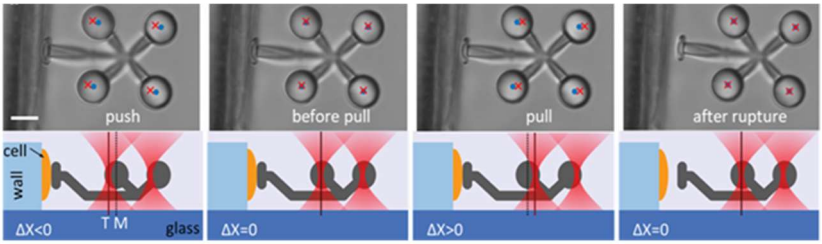

Figure 4. Image sequence from a record of a typical adhesion experiment (the retraction process). The red crosses show the trap positions, and the blue dots mark the centers of the microtool's spherical handles; scale bar: 5µm. Below each image a corresponding schematic side view drawing shows the relative positions of the trapping beam and the microtool. The dark red line shows trap position (T), the black dotted line that of the manipulator sphere's center (M)

5. Data evaluation

5.1. Cell stiffness measurements evaluation

The position of the micromanipulator on every video frame recorded during the approximation of the endothelial cells was determined with a correlation-based method where the reference was the image taken at the first position. The four spheres' positions were determined independently, by choosing a template image for each spheres which was a cropped image of the chosen sphere on the very first frame; this chosen reference image was then compared to the image of the same sphere on all other frames of the recording. The resulted correlation matrix has a maximum at the vicinity of the location of the sphere, but it is determined only with one pixel precision (which is in our case 120 nm). To obtain sub-pixel precision position for the spheres, the neighborhood of the matrices' maximum was fitted with a 2D Gaussian function. Afterward, the position of the manipulator's tip was determined from the spheres position data with simple geometric considerations assuming a rigid structure. The main reason why not the tip itself was monitored is that after it makes contact with the cell's surface the image became distorted, and it was cumbersome to apply cross-correlation on it.

The evaluation resulted in tip position vs. trapping focus position traces for every indentation experiment, having two distinguishable ranges. One describes the movement before the contact happens between the microtool and the surface; in this range the manipulator follows the trap position continuously/precisely, and its slope is 1. After the structure made the contact, it lags the traps position so the slope in this range is less than 1. We had two distinct set of traces, one for the cell indentations and another for the wall approach experiments. In both set of traces a reference trace was selected and the other traces were aligned to it in a subsequent alignment procedure.

5.2. Adhesion force measurements evaluation

The recorded image sets were analyzed by a Matlab program for the adhesion-force measurements as well. At all images from one adhesion force measurement, the program fits a circle for all four spheres of the used micromanipulator, and the centers of these circles are considered as the trapping sphere centers for each sphere. The average position of the four centers of the spheres was then calculated and its coordinate along the direction of the movement of the optical trap was plotted as the function of the holding foci`s position.

The ΔX displacement values for the optical force curves during the retraction process were determined in the following way. As long as the microtool is attached to the cell, its position is constant. After its detachment from the cell (with or without adhesion) in each individual

measurement, the averaged sphere center positions coincided with the position of the trapping beams and grows linearly with it (*Figure 5/c* grey dots). A straight line was fitted to this linearly rising section, which was extrapolated to zero trap position and the averaged sphere position was subtracted from it, resulting the ΔX values (*Figure 5/c* red dots).

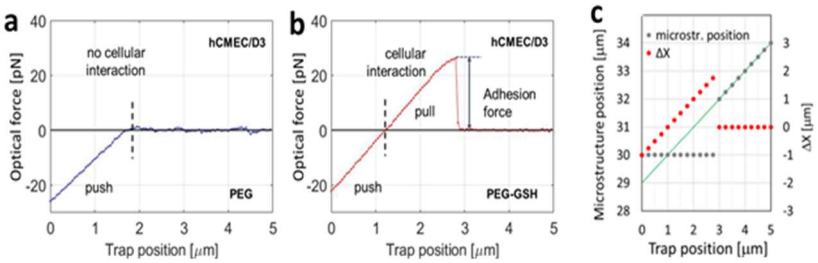

Figure 5. ***(a)*** *and* ***(b)*** *shows a typical adhesion force measurement plots for* ***(a)*** *a PEGylated and / control functionalized* ***(b)*** *GSH-coated microtool on D3 cells with 50 nm stepsize which shows a strong cellular interaction, part* ***(c)*** *Illustrates the determination of ΔX from the microtool position as the function of the trapping focus position (0 refers to the start of the pulling of the microtool). Grey circles show modelled microtool positions along the direction of the retraction in the image coordinate system. In this example, in the 0-3 μm trap position ranges the manipulator does not move due to its adhesion to the cell`s surface. At 3 μm it detaches from the cell and above 3 μm it precisely follows the trapping beam. The grey line is the fit to this last, 3-5 μm section. ΔX is calculated by subtracting the microtool positions from the fitted line*

The optical force was simply calculated by multiplying the ΔX values with the previously measured stiffness of the microtool (k_{str} = 25.8± 2 pN/μm). The adhesion force is the amplitude of the sudden drop of the optical force which is the result of the rupture in the adhesion between the structure and the cell`s surface (*Figure 5/b*).

III. Results and discussion

1. Determination of endothelial cells Young`s modulus

The endothelial cells Young's modulus was calculated based on the Hertz model which is one of the most widely used methods in the literature for AFM and OT indentation experiments.

The forces and the indentation were determined from the microtool's position as the function of the trapping beams position. After the contact of the microstructure and the cell, the movement continues to be primarily a linear function of the trapping beams position for at least another 500–800 nm of trap movement; in this regime, the tip moves less than 150 nm. Infrequently, the tip slips sideways on the cell membrane even by about 100 nm. Average of traces from

approximations of the SU-8 scaffolds with no cells on them (control experiment, red curve) and one aligned tip position trace when pushed against a cell (green curve) is shown on *Figure 6/b*.

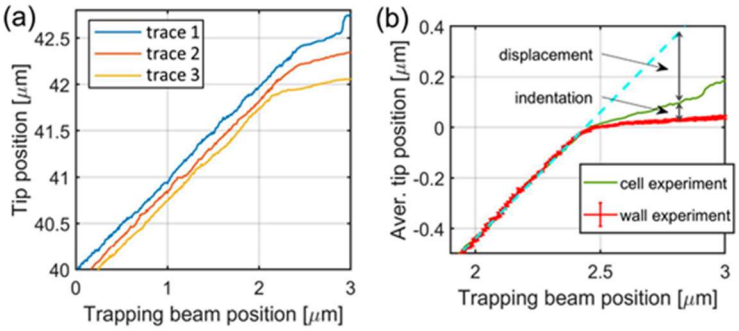

Figure 6. Tip position traces for the calculation of endothelial cell's Young's modulus. ***(a)*** *shows representative raw tip position traces as the function of the trap positions before alignment. After the alignment procedure, the tip positions* ***(b)*** *of the wall approach experiments were averaged for background (red curve), while the cell indentation traces (the green curve)*

Since the tip can slip sideways, the tip position is mainly meaningful in the first 400 nm after the contact point, where this effect is negligible. This effect could be observed when a tip was pushed against the SU-8 wall, and therefore the tip has a residual forward movement after the contact point. Since this may also happen in the cell experiments, the observed extra forward movement at the walls was used as a correction in the cell indentation measurements (the tip positions of the cell experiments were compared to this baseline). On *Figure 6/b* two typical position traces are illustrated which were used to determine the indentation forces in the Hertz model for each individual measurement. The difference between the tip position when approaching the wall and when approaching the cell gives the indentation. A straight line was fitted to the linearly increasing part of the cell approach trace (*Figure 6/b* cyan dashed line) and the difference between this and the tip position trace after the contact point was used to calculate the displacement. The indentation force was determined from the displacement by multiplying it with the stiffness of the microtool (k_{str}); the resulted force ranged between 1-5 pN, which transcends the AFM precision. Both the indentation and the displacement traces have a break point at around 2.5 μm, but about 400 nm beyond the contact point they produce large errors. Therefore, the Young's modulus could be obtained reliably from the range of 2.5–2.9 μm. *Figure 7.* shows that the obtained values range from 220 Pa up to 1500 Pa, but between 2.5-2.6 μm trap positions (indentation between 0.01 μm and 0.02 μm) the determined values have significant noise. The

obtained data was recorded with 4 microtools on 6 cells, altogether 19 measurements was carried out.

These measured values are parallel with those determined by AFM-based methods on endothelial cells from pulmonary artery with a modulus of 400–1500 Pa, on bovine aortic endothelial cells with 700-2700 Pa, with another technique based on magnetic tweezers with 400 Pa. Interestingly those values which were achieved with AFM, the moduli can vary an order of magnitude for the same type of cell in the literature. The most possible reason for this broad range could trace back to the measurement conditions: the rate and amount of indentation and the indenter tool's shape. In the literature it was demonstrated that the indentation rate increases the Young's modulus mainly due to viscous effects and that about 0.25 µm/s probe velocity was the lower limit of viscous dissipation. Our OT-based measurements take about one minute each, and it is only about the last sixth of the measurement, where the tip reaches and indents the cell with about 60 nm; by the end of this period, the force increases to about 6 pN, what corresponds to 1 pN/s loading rate and the indentation rate of 0.01 µm/s which is much smaller than those for AFM. In our experiments due to the low indentation rate, we consider the viscous effects negligible in measuring the Young's moduli.

Furthermore, when the amount of indentation is too large, the intracellular actin network could spoil the measurement of the elastic properties of the cell membrane. The relatively large noise observed for small indentation values were very likely produced by the thermal fluctuation of the trapped microtool, when small indentations and forces are applied. Although the optical force of our presented experiments together with the 300 nm tip radius of the microtool yielded the indentation values of up to 90 nm, our operating range can be easily increased to greater values with higher trapping laser intensity and smaller trapping sphere diameters.

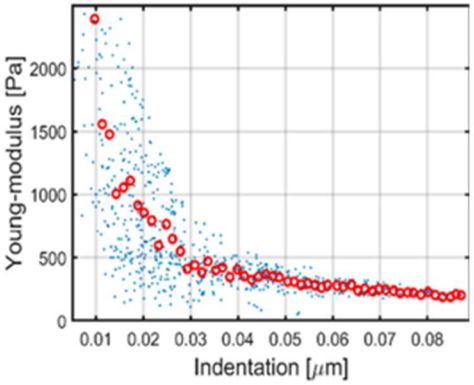

Figure 7. All measured Young's modulus of D3 cells. The blue dots represent all the approximately 800 individual point pairs (40 trap positions × 19 experiments), while the red circles are their averages in 60 regions over the 0–0.09 µm indentation range.

2. Calculation of GSH coverage on SU-8 surface

To obtain the surface coverage of GSH on SU-8, first we determined the integrated fluorescence intensity of single CY-5 molecules (*Figure 8/a*) with the methodology detailed in the Methods section of my thesis. The integrated fluorescent intensity of the image of a single CY-5 fluorophore was measured to be 200±39 pixel intensity unit (n=71) (*Figure 8/b*). The determined average fluorescence intensity for each pixel (where a sample area of 100 nm x 100 nm was imaged) on the GSH functionalized sample was 6727±349 (n=7) and on the PEGylated sample 1794±224 (n=21). The difference pixel intensity value between the GSH functionalized and the PEGylated one was integrated over one μm^2 and the result was divided by the integrated intensity of a single CY-5 molecule, what gave us 2464±770 molecule/μm^2 surface coverage value. Supposing that each GSH binds one fluorophore molecule, this results in approx. 2500 GSH molecules on every square micrometer on the surface of the SU-8 structures

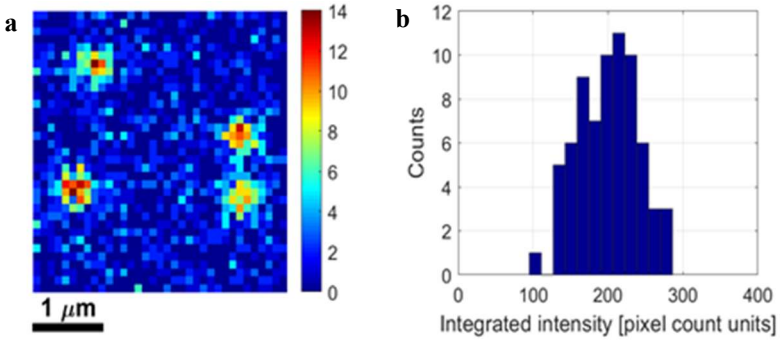

*Figure 8. The integrated intensity determined from the fluorescent images of single CY-5 fluorophore molecules **(a)** were used to calculate the surface coverage of CY5 on the homogeneously coated layers (the colorbar shows fluorescent intensity in pixel count units). The intensity of the single dye molecules was quite uniform, giving a well-defined average integrated intensity value **(b)** (N=71).*

3. Binding probability on different cell types

Before I made the binding measurements, I've done preliminary experiments with simple ellipsoids made by TPP fabrication on 4 types of cells: primary rat brain endothelial cells (RBEC), human endothelial cell line (hCMEC/D3), primary rat brain astrocytes and pericytes to shed light on the binding probability between them and PEGylated and PEG-GSH functionalized SU-8 surfaces (cells were grown on a horizontal glass surface instead of a vertical wall). We expected that the GSH coated ellipsoids can reach a better binding ratio than the control functionalized

(PEGylated) ones on the different cells. For each cell type we made at least 2 series of binding attempts on different cultures and days.

A binding attempt was carried out as follows: an individual, previously functionalized (either PEGylated or PEG-GSH) ellipsoid was picked up by the optical tweezers, and was pushed to the cells surface nearby the nuclei, but far enough to have a planar surface. It was pushed against the cell for 10 seconds and after that the optical tweezer was slowly moved upwards to remove the ellipsoid from the cell. This could end with binary outputs: if there was not enough adhesion between the cell and the ellipsoid, then it can be removed from the cell membrane (**non-bound event**); if there was enough adhesion, the structure could not be removed by optical forces (**bound event**). At *Figure 9*. the ellipsoid binding experiments results are shown, whit the representing element number and the binding probability in terms of percentage (bound events divided by all) at the top of each column. A clear distinction could be observed between the binding probabilities of the PEG-GSH functionalized ellipsoids relative to the PEGylated (control) ones for all 4 cell types.

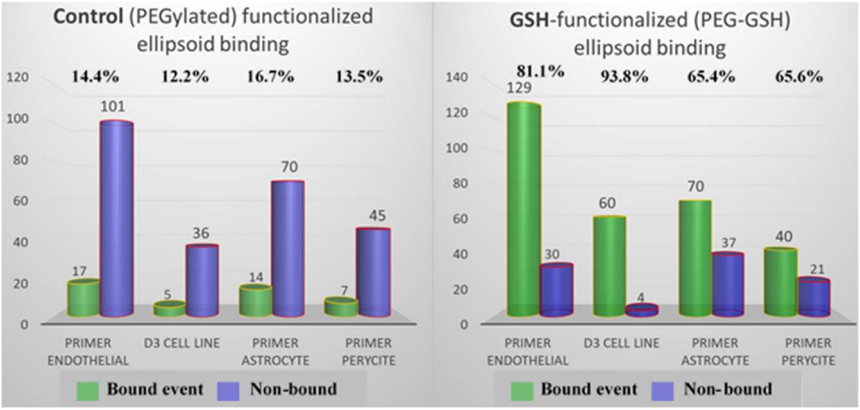

Figure 9. Ellipsoid binding experiments on four different cells, at the left side the PEGylated ellipsoids binding probabilities are show, ant the right the same for PEG-GSH functionalized ones

After these experiments I was convinced, that in the final adhesion force measurements pericytes and astrocytes cannot be used, because they grew in a random 3D structure which would make it very hard to reach them on the SU-8 walls. The other two endothelial cells have more 2D shapes flattened to the surface of the substrate, therefore they can be approached easier with the microtools. When GSH was present on the surface, the ellipsoids bound to primary endothelial cells with 81% probability as compared to 14% in the absence of it. Similar results were observed with hCMEC/D3 cells where GSH-coated ellipsoids reached 93% binding probability versus only

12% in the control functionalized ones where the GSH missing. Hereinafter we made corresponding AFM measurements with sharp silica tipped cantilevers either PEGylated or GSH functionalized ones on hCMEC/D3 cells which gave similar results as we observed during the ellipsoid binding probability experiments.

4. Adhesion force measurements of GSH functionalized structures

For these measurements TPP-made and optically manipulated microstructures were used with flat contact surface (shown in *Figure 1/a*), and the cells were cultured on a vertical scaffold-like supporting wall. We carried out at least two individual measurements with each cell type and functionalization parameters on different cultures and days. The retraction of the micromanipulators in a well-controlled manner by stepping the trapping foci after they were pushed against the cell's surface has a capital importance in these measurements. These retractions were made with two different step sizes, namely 50 and 250 nm which represents the following retraction speeds: 0.1 μm/s and 0.5 μm/s respectively. If there was adhesion between the microstructure and the cell, the pushing force switches to pulling during the retraction, otherwise the manipulator detaches from the cell membrane and no pulling force acts on it. When there was adhesion, the cell membrane was pulled by the microstructure up to a particular trap position, where the bond between the two surfaces ruptures and they detach from each other, returning the optical force to zero. The optical force at the rupture position defines the adhesion force (*Figure 5/b*). Curiously, we did not find any correlation between the initial pushing force and the magnitude of the adhesion force.

All adhesion force traces for GSH and PEGylated micromanipulator measurements shown on *Figure 10/a, b* were obtained using one applied stepsize and cell type. I observed that the

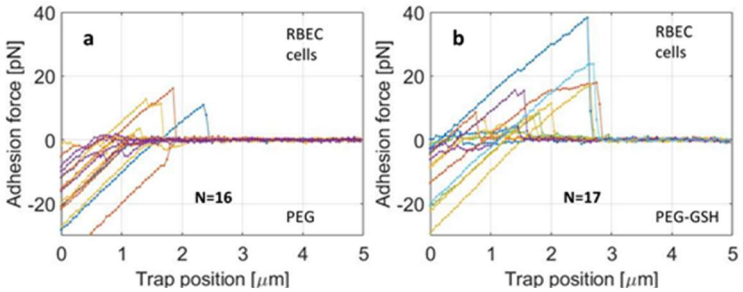

*Figure 10. Adhesion force curves from all experiments on **(a, b)** rat brain endothelial cells (RBEC) made with 50 nm stepsize*

adhesion force means were always significantly greater when GSH was present than when it was

omitted, and the ratio of the average measured adhesion forces between the two functionalization groups could be as high as eight. In case of the GSH-coated structures, the difference between the 50 nm stepsize values and those recorded with 250 nm stepsize was not found to be statistically significant.

With 250 nm stepsize, we measured 9 ± 6.6 pN adhesion force for RBEC cells and 16.4 ± 6 pN for hCMEC/D3 cells when the targeting ligand GSH was present, while for PEGylated microtools the adhesion forces were only 2.2 ± 3 pN for RBEC and 2 ± 4.3 pN for hCMEC/D3; the element numbers are shown on the graphs of the individual force curves When the smaller stepsize was used, the average adhesion force for GSH functionalized microtools was 12.1 ± 9.5 pN on RBEC cells and 10.2 ± 7.2 pN on hCMEC/D3 cells, whereas in case of the PEGylated microtools, our control group, it was 3.4 ± 4.9 pN RBEC and 3.8 ± 3.2 pN for hCMEC/D3. In case of hCMEC/D3 cells, when the slower speed was applied, we observed large plateau like curves.

When the smaller stepsize was used, the average adhesion force for GSH functionalized microtools was 12.1 ± 9.5 pN on RBEC cells and 10.2 ± 7.2 pN on hCMEC/D3 cells, whereas in case of the PEGylated microtools, our control group, it was 3.4 ± 4.9 pN RBEC and 3.8 ± 3.2 pN for hCMEC/D3. In case of D3 cells, when the slower speed was applied, we observed large plateau like curves.

We performed experiments with similarly GSH functionalized colloidal AFM cantilevers where a 5 µm radius spherical bead was attached at the tip of it (*Figure 11/c*, inset); we chose this special cantilever because it has a comparable contact surface with our microtool. The AFM measurements resulted in 3-6 times greater adhesion forces than those obtained with the HOT method both for RBEC cells (38±18 pN), and for hCMEC/D3 cells (57±28 pN) (N=247 for both cases). The most possible reason why the AFM measurements showed larger adhesion forces is that the AFM probe was pushed against the cell with 100 pN which is almost an order of magnitude higher than in the HOT measurements (there we used only 10-30 pN) what could generate higher number of bonds. On the other hand, the AFM's detection level is around 10 pN, so only those measurements were taken into account which resulted in higher adhesion force than this limit.

The resulted 10-15 pN adhesion force in case of GSH-coated microstructures suggests that it could be a single bond rupture event. Also, the interaction of GSH with the cells seems to be specific, because without it the adhesion was just 2-4 pN. As for the molecular background of the GSH binding to the cells, we believe that the GSH tripeptide's middle cysteine's thiol group is not playing a role in the adhesion because it was used to connect GSH covalently to the PEG-linker's maleimide-group.

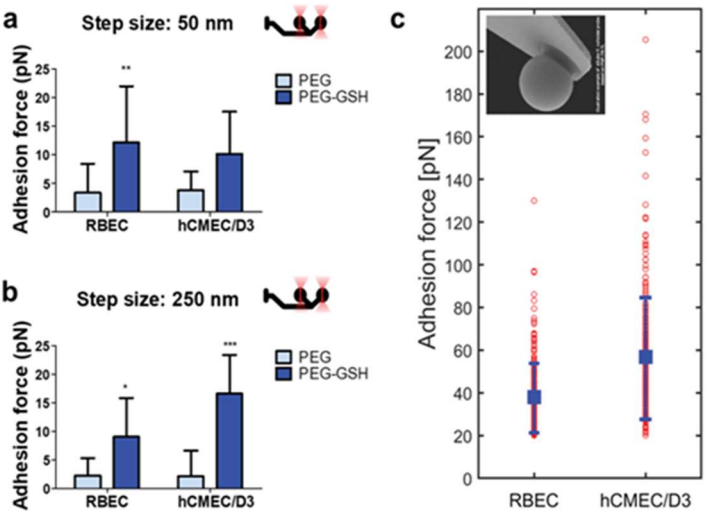

Figure 11. Summarizes the adhesion forces obtained with the GSH and with the PEGylated microtools on brain endothelial cells using two step sizes ***(a)*** *and* ***(b)*** *Values presented are means ± SD. Statistical analysis: ANOVA* ***(c)*** *Adhesion force between PEG-GSH functionalized colloidal tipped cantilevers and the surface of endothelial cells, as measured with the AFM. Red circles represent individual measurements, blue squares are their means, blue whiskers are SD.*

With our newly developed adhesion force measurement setup, the number of bonds is expected to be presented in larger number in a future experiment, and the applicable optical forces may not be strong enough to rupture them. In this case the functionalization protocol or the microtools contact surface should be fine adjusted. Furthermore, with small changes, our proof-of-concept measurement method can be extended to study dozens of ligands or chemoattractant molecules due to a diverse range of functional PEG-linkers.

4. Conclusion

In my thesis I demonstrated that optical tweezer-based techniques are capable to explore living cells physical and biochemical properties. First, the measurement of Young's modulus of endothelial cells can be carried out with precisely manipulated two-photon polymerized, purpose designed microstructures. Furthermore, the stiffness measurement technique could give very different results depending on the parameters of the experiment: if the pure linear elasticity of the cell is the topic of interest, it is believed that use of indentation surfaces with large radius of curvature and small loading rates as well as small forces is more potent to examine specifically that. Our method is perfectly capable to operate in this range.

In our other work/publication we reported for the first time GSH adhesion forces to brain endothelial cells (hCMEC/D3 and RBEC) using our novel holographic optical tweezer-based binding force measurement technique. In this series of experiments, we used similar SU-8 microtools as in the previous work which could prevent the cells from photodamage. The laser microfabrication made it possible to easily change the geometry of the micromanipulator's probe as the experimental methodology required. In both type of measurement arrangements, we used a cell culturing method where the cells were grown on mask-lithography made walls, which were parallel to the optical axis what enabled us to measure the adhesion force and the stiffness in a direction perpendicular to the cell membrane by approximation of the cell via lateral movement of the trapped microstructure.

We measured adhesion forces in the regime of 10-15 pN when the GSH was present that indicates a specificity towards glutathione: when void of the targeting ligand (PEGylated structures) we observed notably, 3-8 times smaller forces. The adhesion forces what we observed coincide with those what could be found in the literature for other receptor ligand pairs also measured with optical trap-based methods. Our method could be extended in the future to differentiate between multiple and single binding events, to characterize other BBB targeting ligands with the adhesion force on living cells or even to select novel targeting molecules. The functionalization protocol could be easily adapted to immobilize those molecules with covalent bonds, thanks to the variety of PEG-linkers.

List of publications

MTMT identification number: 10061212

Cumulative impact factor: 19.19

Publications related to the subject of the thesis:

I. **Tamás Fekete**, Mária Mészáros, Zsolt Szegletes, Gaszton Vizsnyiczai, László Zimányi, Mária A. Deli, Szilvia Veszelka, Lóránd Kelemen; Optically manipulated microtools to measure adhesion of the nanoparticle targeting ligand glutathione to endothelial cells; *ACS Applied Materials & Interfaces*; 39018-29 Vol. 13, (2021); IF: 9.23

II. István Grexa, **Tamás Fekete**, Judit Molnár, Kinga Molnár, Gaszton Vizsnyiczai, Pál Ormos, Lóránd Kelemen; Single-Cell Elasticity Measurement with an optically Actuated Microrobot; *Micromachines*; 2072-2085: 11 9 Paper 882. 13 p. (2020); IF: 2.89

Articles not related to the thesis:

I. Gaszton Vizsnyiczai, András Búzás, Aekbote Badri Lakshmanrao, **Tamás Fekete**, István Grexa, Pál Ormos, Lóránd Kelemen; Multiview microscopy of single cells through microstructure-based indirect optical manipulation; *Biomedical Optics Express* 11: 2 pp. 945-962, 18 p. (2020); IF: 3.73

II. Aekbote Badri Lakshmanrao, **Fekete Tamás**, Jacak Jaroslav, Vizsnyiczai Gaszton, Ormos Pál, Kelemen Lóránd**;** Surface-modified complex SU-8 microstructures for indirect optical manipulation of single cells**;** *Biomedical Optics Express* (2156-7085): 7 1 pp 45-56 (2016); IF: 3.34